

Affordable retrofitting methods to achieve thermal comfort for a terrace house in Malaysia with a hot-humid climate

Tuck, Ng Wai

Malaysia-Japan International Institute of Technology, Universiti Teknologi Malaysia

Zaki, Sheikh Ahmad

Malaysia-Japan International Institute of Technology, Universiti Teknologi Malaysia

Hagishima, Aya

Interdisciplinary Graduate School of Engineering Sciences(IGSES), Kyushu University

Rijal, Hom Bahadur

Department of Restoration Ecology and Built Environment, Tokyo City University

他

<https://hdl.handle.net/2324/4795144>

出版情報 : Energy and Buildings. 223, pp.110072-, 2020-09-15. Elsevier
バージョン :
権利関係 :



1 Affordable retrofitting methods to achieve thermal comfort for a
2 terrace house in Malaysia with a hot–humid climate

3 Ng Wai Tuck^{a,b}, Sheikh Ahmad Zaki^{a*}, Aya Hagishima^c, Hom Bahadur Rijal^d, Fitri Yakub^a

4 ^a Malaysia–Japan International Institute of Technology, Universiti Teknologi Malaysia, Kuala Lumpur, Malaysia

5 ^b School of Architecture, Faculty of Built Environment, Tunku Abdul Rahman University College, Kuala Lumpur, Malaysia

6 ^c Interdisciplinary Graduate School of Engineering Sciences, Kyushu University, Japan

7 ^d Department of Restoration Ecology and Built Environment, Tokyo City University, Yokohama, Japan

8 *sheikh.kl@utm.my

9

Highlights

- Natural ventilation alone was not sufficient to achieve thermal comfort.
- Natural ventilation assisted with retrofitting methods are better solution.
- A roof cover reduced convective fluxes by 70–80% in attic and 88% in room.
- The use of the roof cover is a zero-energy-consumption low-cost affordable method.
- Assisted air ventilation with ceiling fan improve thermal comfort effectively.

Abstract

Although various cooling approaches have been proposed to overcome the thermal discomfort in residential buildings, tropical developing countries still lack affordable and effective retrofitting methods. The objective of this study was to evaluate the effectiveness of an affordable retrofitting method with high-density polyethylene (HDPE) nets as roof covers for shading over the roof, supported by full day free-running ventilation, and heat insulation above the ceiling of residential buildings in hot–humid climate regions to overcome the thermal discomfort. Field measurements were carried out in a corner terrace house in Malaysia, from September to December 2018. The roof cover with HDPE nets maintained a consistent surface temperature at the roof tiles and reduced the convective heat flux by approximately 70–80% in the attic and 88% in the room. Further, it improved the compliance (acceptability: 80%) of the whole-day mean operative temperature in the room (hot–humid climate) by 10%. The roof cover can effectively provide thermal comfort in residential buildings in Malaysia, which has a hot–humid climate. Alongside active cooling with the ceiling fan, required comfortable indoor temperature can be reached under the hot–humid climate, particularly during the night-time. Furthermore, the zero-energy-consuming, low-cost low-technology roof cover method is very suitable for low-cost houses with roof tile in hot–humid climate regions.

Keywords: passive cooling, building retrofitting, free running ventilation, roof cover, thermal comfort

Abbreviations

ACE	-	Adaptive thermal comfort equation
ASHRAE	-	American Society of Heating, Refrigerating and Air-Conditioning Engineers
CFD	-	Computational Fluid Dynamics
EN	-	European Standard
NV	-	Full day natural ventilation
NV-R	-	Full day natural ventilation with retrofit roof cover
NV-R-C	-	Full day natural ventilation with roof cover and heat insulation above ceiling.
NV-R-C-F	-	Full day natural ventilation with roof cover, heat insulation above ceiling, and mechanical ventilation with ceiling fan.
HDPE	-	High density polyethylene
PV	-	Photovoltaic

1. Introduction

According to the United Nations [1], the electricity consumption corresponded to 19% of the total world energy consumption, 27% of which was used by households. Most of this energy consumption goes towards heating and cooling the residential buildings. The use of energy for building cooling exhibits the highest increase rate. According to a report by the International Energy Agency [2], the share of cooling in the total energy use in buildings has increased from approximately 2.5% in 1990 to 6% in 2016. For tropical countries such as Malaysia, in 2016, 11% of the electricity in the residential sector was consumed for space cooling [3], and the energy consumption was effected by outdoor weather conditions [4]. This fraction is expected to increase owing to the increasing demand for air conditioners, economic growth, and climate changes.

1.1 Literature review

In recent years, smart-house technologies consisting of various energy-efficient appliances, roof-top photovoltaic (PV) solar panels [5,6], and home energy management systems [7] have attracted attention for the provision of energy-saving, low-carbon comfortable indoor environments. However, such advanced technologies are not affordable for most developing countries in equatorial regions. As a more economical option, building retrofit strategies without the use of energy has attracted attention as an effective method to overcome the thermal discomfort [8–13]. Retrofitting of existing buildings offers significant opportunities for reducing energy consumption towards nearly zero energy levels [13,14] and is being considered as one of the main approaches to achieving sustainability in the built environment at a relatively low cost [12].

Tuck et al. [15] performed a field experiment on the indoor thermal environment of a terrace house in Malaysia and pointed out that free-running ventilation was not adequate to provide comfortable indoor thermal comfort without assistance from mixed-mode ventilation. The outdoor thermal environment significantly influenced the effectiveness of free-running ventilation. Ivan [16] found that building colour, shading system, night ventilation, controlled ventilation, roof coating, and eco-evaporative cooling are the most suitable retrofitting methods for extensive use in Mexico with a tropical climate. Lan et al. [17] found that natural ventilation with louvre windows offer a 32% improvement of thermal comfort in patient wards in Singapore.

Houses in equatorial regions are exposed to large radiant heat gains at roofs due to higher solar altitudes during the day-time. The absorbed solar radiation (SR) by the roof is transported towards the interior space through conduction, convection, and radiation [18]. Heat gain from the roof contributed 70% of total heat gain in tropical houses [19]. A field study by Toe and Kubota [18] on a two-storey modern terrace house in Malaysia demonstrates that the surface temperature of the ceiling beneath the roof recorded the highest value during day-time that was 2.7 °C higher than the room air temperature. The daily maximum heat flow through the ceiling into the room was approximately 33.9 W/m² in the day-time [18], indicating that the large radiant heat gain at the roof contributed to the increase in indoor temperature. Tuck et al. [15] found that the primary source of heat gain in the top-storey rooms of a two-storey house was from the ceiling surface below the roof. The vertical distribution of the room air temperature exhibited a gradual increase towards the ceiling. Thus, the reduction in heat gain at the roof from the high SR is a key approach to decrease the room air temperature of a low-rise building in the equatorial region.

Passive cooling through retrofitting techniques by using reflective and radiative roofs in tropical houses can decrease heat gain by facilitating the elimination of excess heat in a building's interior to maintain a comfortable environment [19]. Double-skin roof (two roof layers with an air gap between them) can be used to modulate the roof heating by SR [20]. The outer layer acts as a reflector or absorber of the SR, while the second layer covers the internal spaces [20]. The air gap between the two layers acts not only as insulation but also as an effluent pathway for the heat absorbed by the outer layer to move outwards under a tropical environment [20]. The double-skin roof reduces the heat gain by up to 71% in buildings in Singapore with a tropical climate [21]. The efficiency of a double-skin roof was increased by up to 85%, with an outer layer having high reflectivity in Djibouti City (hot arid climate) [22]. The performance of a double-skin roof was 28–34% higher than that of a normal single-layer-insulated roof for the reduction in heat gain into the building during day-time in Singapore [23].

Recent studies demonstrate that using PV panels as the outer layer of a double-skin roof can be an effective retrofitting method, which not only functions as a shading device but also absorb heat and convert it to electrical energy for usage or supplying back to the grid system [20,24,25]. The reduction in heat flux gain through the roof can be 60–63% [5], compared to that of an exposed roof. The estimated energy saving on the cooling load was approximately 6–7% for a building installed with a PV in Thailand in the tropical zone [6]. Although the rooftop PV promises to achieve an approximately zero net energy house [26], it is challenging to widely implement this approach in developing countries

owing to its high price. For example, the cost of installation of a PV system in Malaysia in 2019 was estimated to be 1075–2030 USD/kW [27], which is equivalent to 64–122% of the mean monthly household income in Malaysia in 2016 [28].

On the other hand, as an alternative, various fabrics have been extensively used for shading in the building [29] and agriculture [30,31] sectors. Kachkouch et al. [29] evaluated the influence of a fabric sheet, used for shading the roof, for cooling and reported a reduction in ceiling temperature of 8.9 °C. Soni et al. [31], investigating the thermal effects of high-density polyethylene (HDPE) nets as greenhouse barriers to protect plants from the intensive SR, reported that the effect of shading could be controlled by the different percentage of openings in the nets. Although such fabric shading devices can be regarded as makeshift attachments rather than static building structures, the fabric shading on roofs is expected to be an affordable, effective retrofitting strategy in tropical developing countries, particularly for low-rise buildings such as single- and double-storey terrace houses.

In addition to the reduction in heat by a double-skin roof, the installation of a heat-insulation layer in the attic under the roof is an alternative method applied in tropical regions [20]. The insulated roof could reduce heat transfer through the ceiling by 80–90% [32]. By experimentally assessing the thermal performance of an insulated roof, Kachkouch et al. [29] demonstrated that the air temperature in the test cell reduced by 9.9 °C.

Although it is widely known that solar heat gain through the roof is considerable in low-rise terrace houses [18–20,32] and solar shielding of the roofs [21,22] could reduce the primary heat gain in low-rise buildings, this common knowledge has not been implemented as affordable design for residential buildings in many developing countries, particularly low-cost houses, suggesting a knowledge gap between the academic community, the construction industry, and the policy makers.

1.2 Objective of the study

The objective of this study is to propose an affordable retrofitting method to improve the indoor thermal environment of low-cost low-rise buildings in hot-humid climate regions. It is an extension of the study done by Tuck et al. [15] on the effectiveness of free-running passive cooling strategies for indoor thermal environments on a real two-storey corner terrace house in Kuala Lumpur, Malaysia.

2. Materials and methods

2.1. Location and climate

The field measurement was carried out in a two-storey corner terrace house (Fig. 1a) in Taman Melati, Kuala Lumpur, Malaysia ($3^{\circ}13'10.3''$ N $101^{\circ}43'33.9''$ E), from 2nd September to 16th December 2018. Kuala Lumpur is located in the equatorial region and has a tropical rain forest climate throughout the year. Terrace houses are the main type of living quarters in Malaysia and amount to 36.4% of the total living quarters in Malaysia [33]. Furthermore, in 2018, terrace houses propelled the new launches of residential property in Malaysia, accounting for 47.8% of the market volume [34]. Fig. 1b shows the monthly mean outdoor air temperature of Kuala Lumpur in the period of January to December 2018, obtained from a weather station at Universiti Teknologi Malaysia, Kuala Lumpur campus, approximately 5 km away from the investigated house. The setup of the weather station was presented by Swarno et al. [35]. The mean outdoor air temperature and relative humidity (*RH*) were 28 ± 2 °C and $80 \pm 7\%$, respectively. The results are similar to those reported by Khalid et al. [36] on the monthly mean outdoor temperature and *RH* variations throughout the year.

2.2. Investigated house

The total built-up area of the house was approximately 178 m². The heights of the ground and first floors were 3.0 and 3.2 m, respectively. Floor plans and elevation views of the house are presented in the report by Tuck et al. [15]. Table 1 shows the characteristics of the investigated house.

The construction of the house was completed in 2004 with brick walls on a reinforced concrete frame structure. Table 2 lists the building materials. The material of both floor slabs was reinforced concrete. The top-floor rooms were covered with a cement board ceiling and concrete roof tiles (Fig. 2). The *U* values of the ceiling board and roof tiles were high at 66.7 [37] and 70.8 [38] W/(m²·K), respectively. According to the manufacturer [37] of the ceiling board, the thermal conductivity is 0.3 W/m.K, and the thickness is 4.5 mm. With such a thin sheet of ceiling board, the *U* value is expected to be high. As expected, the *U* value is also high (70.8 W/(m²·K)) for the roof tiles that are made of

concrete having a thermal conductivity of 0.85 W/m.K, and a thickness of 13 mm. Notably, no insulation layer was incorporated in the envelope of the house, including floors, walls, roof tiles, and ceilings.

2.3. Measurement

Measurement was carried out in the master bedroom on the top floor, owing to its west-facing orientation and highest temperature in the investigated house [15] as continuity from the previous study. There were no occupants in the room during the period of measurement to eliminate any influence of human factors to the measurement. All windows of the room were fully open during the measurement to allow completely natural ventilation in the room while its door was closed. Four cases with different combinations of natural ventilation, passive cooling, and active cooling strategies were considered (Table 3). The process of measurement for four cases is shown in Fig. 3. The measurement in each case was carried out for five consecutive days, with intervals of approximately 20 to 30 days for the installation of retrofitting devices and materials. The whole measurement period was three months (September to December 2018).

The first case was based on full day natural ventilation (NV) through the windows as a reference for comparison to the other cases. The second case (NV-R) involved full day NV and fabric roof shading, proposed by Abuseif and Gou [20], attached to the existing roof. This was performed to check the effectiveness of roof cover using HDPE nets to reduce heat gain on the roof. In the third case (NV-R-C), an insulation board consisting of fibre glass was installed above the ceiling board of the master bedroom on the top floor in addition to the NV-R setting. The addition of heat insulation board above the ceiling is to enhance the blocking of heat gain through the roof by having a second layer of filter to the penetration of heat. In the fourth case (NV-R-C-F), active cooling with a ceiling fan was used in addition to the above three strategies to improve natural ventilation by enhancing air movement in the room, as highlighted by Tuck et al. [15]. In Malaysia, ceiling fan is the common fitting in the house for ventilation purposes. Most people will switch on the ceiling fan on hot days and during night time during sleeping.

2.4. Measurement setup

2.4.1. Instrumentation

The outdoor air temperature (T_o), relative humidity (RH_o), and wind speed (V_o) were measured in the open space beside the house [15]. Outdoor air temperature and relative humidity were measured at 1.5 (human height at the ground floor), 3.0 (height of the first floor), and 4.5 (human height at the first floor) m from the ground level to evaluate the outdoor vertical temperature profile. The external sensor was housed in a fan-aspirated solar shield to avoid the effect of the solar radiation. Simultaneously, solar radiation was measured at 4.8 m above the ground, while wind speed was measured at 5.0 m above the ground. The indoor air temperature (T_i), relative humidity (RH_i), globe temperature (T_g), and air velocity (V_i) were measured in the master bedroom. Fig. 4 shows the measurement points (plan view; Fig. 4a) and types of climatic parameter measurements (cross-section view; Fig. 4b) in the master bedroom and roof.

Fig. 5 shows the setup for each measurement. Indoor air temperature and relative humidity were measured at three different heights (0.5, 1.5, and 2.5 m) in the investigated areas (Fig. 5a) to represent the thermal environment above the floor, in the middle of the room, and below the ceiling. Indoor globe temperature and air velocity were measured at 1.5 m above the floor. The attic air temperature was measured at 0.8 m (1/3 of the attic height) and 1.6 m (2/3 of the attic height) above the ceiling level at the centre of the roof attic (Fig. 5b) to obtain the vertical variation in air temperature between the roof tiles and ceiling. The surface temperature of the roof tiles was measured at the bottom surface of a roof tile above the master bedroom (Fig. 5c). Simultaneously, the temperatures of the top and bottom surfaces of the ceiling board (Fig. 5d and 5e) were measured. The instruments used in these field measurements are listed in Table 4. All indoor and outdoor instruments recorded values at intervals of 1 min. The consistent readings of all instruments were verified before the measurements by comparison of their measured values.

2.4.2. Retrofitting of a roof cover

A layer of black HDPE net with 90% shading (low transmittance and high absorptance on solar radiation) was set on top of the existing roof as a roof cover (Fig. 6) in all cases except for case NV. The net was supported with a timber frame (Fig. 6a and 6b). An air gap (thickness: 300–600 mm) was provided between the existing roof and roof cover to allow ventilation for cooling. The net was supported on a $1 \times 1 \text{ m}^2$ grid timber frame (Fig. 6b) placed directly on top of the existing roof (Fig. 6c). In addition to the measurement of the indoor thermal environment (section 2.4.1), the surface temperature of the roof cover, temperature of the air gap, surface temperature of the covered roof tile (Fig.

6e and 6f), and surface temperature of the uncovered roof tile of the neighbouring house (Fig. 6d) were recorded as additional data in case NV-R.

2.4.3. Retrofitting of an insulation above the ceiling

Fig. 7 shows a 50-mm-thick Rockwool slab with a density of 60 kg/m³, used as the heat insulation between the attic and rooms in cases NV-R-C and NV-R-C-F. It was set horizontally above the ceiling boards above the master bedroom.

2.4.4. Mechanical assisted enhance air movement with the ceiling fan

In case NV-R-C-F, the speed of the ceiling fan at the centre of the master bedroom (Fig. 8a) was set to 2 (Fig. 8b), which is the normal speed set by the owner of the house and is equal to approximately 165 m/min (estimated from product specification for ceiling fan of 1500mm diameter), throughout the five days of measurement to assist in room ventilation.

3. Results and discussion

3.1. Outdoor climatic conditions

The outdoor climatic variables, SR , T_o , RH_o , and V_o , were converted to hourly averaged data and plotted against time (Fig. 9) for the four cases. In general, the outdoor climatic conditions were different among the four cases. As the target site was located at the equator, the times of sunrise and sunset during the measurement were fixed (7:00 and 19:00, respectively). We could estimate the weather on each day by the diurnal variation in solar radiation. Among the four cases, the numbers of days having solar radiation larger than 800 W/m² were not equal. Table 4 lists the average hourly solar radiation values and average daily outdoor air temperature for the measurements for five days of the four cases. The underlines indicate the days in the different cases having approximately equal solar radiation values. The last two days, in case NV, exhibited smaller solar radiation values owing to the heavy rain in the afternoon.

In addition, cases NV-R and NV-R-C-F had smaller solar radiation values than those of the other two cases. The outdoor air temperature also differed between the four cases; the days with smaller solar radiation values tend to have lower outdoor air temperature values, as expected. Fig. 10 shows the outdoor wind speed and wind direction for the four cases. Generally, the wind speed were low in the range of 0.5-2.1 m/s and wind blew from the southeast and southwest directions.

3.2. Indoor thermal conditions

Fig. 11 shows the hourly averaged indoor thermal variables, T_i , T_o , RH_i , and V_i , of the master bedroom. Outdoor air temperature and the temperature difference between the indoor and outdoor, are also included for comparison. Apart from the influence of rain, the indoor temperatures in all cases were in the range of 27 to 33 °C, slightly lower than those in the previous study by Tuck et al. [15] (27–37 °C). As the globe temperature values were similar to the globe temperature values throughout the measurement (Fig. 11a), it can be assumed that a low specific radiation heat existed in the room. The weather conditions differed between the different cases and days. In particular, the fourth and fifth days of NV, the fourth day of NV-R, the fifth day of NV-R-C, and the third day of NV-R-C-F exhibited different trends in temperature differences between the indoor and outdoor (Fig. 11b) owing to precipitation.

On most days in the measurement period, indoor air temperature increased after the sunrise with an increase in outdoor air temperature. However, this increase was modest compared to outdoor air temperature owing to the shelter effect of the building envelopes. Accordingly, indoor air temperature was lower than outdoor during the day-time. The difference between indoor and outdoor air temperature had the largest value (approximately 3 to 5 °C) around noon. In the afternoon, indoor air temperature gradually decreased with the decrease in outdoor air temperature, but the reduction rate was small. Consequently, indoor air temperature exceeded outdoor around 15:00 to 18:00. During the night-time, indoor air temperature was higher than outdoor by approximately 3 to 4 °C owing to the heat storage of the building envelopes, except under heavy rain conditions. The opposite trend was observed for relative humidity. At night, the outdoor air exhibited a higher relative humidity than the indoor for all cases.

The comparison of the different cases for the days with relatively large solar radiation values shows that the daily negative peaks of temperature difference between the indoor and outdoor in the first three days, in case NV without

retrofitting, were 2 to 3 °C, higher than the cases with retrofitting. This implies that retrofitting reduced the room air temperature during the day-time.

Fig. 11c shows that indoor air velocity exhibited a positive correlation with outdoor wind speed in all four cases. Nevertheless, indoor air velocity was very low in all cases without mechanical assisted enhancement in air movement using a ceiling fan (lower than 0.1 m/s), which was not beneficial for improvement in thermal comfort. The low indoor air velocity indicates that the air movement inside the room, created by case NV, was very low even at a moderate outdoor wind speed of 0.2–1.8 m/s. On the other hand, indoor air velocity in case NV-R-C-F with the ceiling fan was increased by approximately 0.2 m/s, compared to the other cases.

3.3. Relationship between the indoor and outdoor air temperatures

To understand the relationship between the daily variations in indoor and outdoor temperatures in the different cases, the decrement factors (f) were calculated as [41]

$$f = (T_{i,max} - T_{i,min}) / (T_{o,max} - T_{o,min}), \quad (1)$$

where $T_{i,max}$ and $T_{i,min}$ and $T_{o,max}$ and $T_{o,min}$ are the daily maximum and minimum indoor and outdoor air temperatures, respectively. Fig. 12 shows the relation between the decrement factor and the daily total solar radiation for each case.

As decrement factor reflects the thermal attenuation of the building envelopes, a building with an airtight super-insulation is expected to have a small decrement factor. In contrast, decrement factor for a building with excessively large ventilation between the room air and outside reaches 1. In our measurement, all four cases involved NV, and the building was thermally improved in terms of solar shading in the four cases. However, no significant differences between the four cases are observed in Fig. 12, probably owing to the short-term gusty rains, which were frequently observed in the afternoon during the measurement period. The typical sudden shower in the tropical region has a small spatial range and transient characteristic. Hence, we could not determine the exact time of the rain by using the precipitation data from the nearest metrological station. Nevertheless, for the days with daily total solar radiation values larger than 15 MJ/day, decrement factor in case NV was larger than those in cases NV-R and NV-R-C, which confirms the effectiveness of the retrofitting for the reduction in heat gain.

3.4. Comparison of the vertical temperature profiles in the master bedroom

The vertical profiles of the air temperature, from the floor of the master bedroom to the rooftop, are shown in Fig. 13. The presented values are the relative temperatures with respect to the floor of the master bedroom, time-averaged over the entire period, including the day-time (7:00 to 19:00) and the night-time (19:00 to 7:00). The temperature of the roof surface of the neighbouring dwelling directly exposed to the atmosphere is included for reference.

In the case NV, the room air temperature gradually increased with the height, during both night- and day-time. In contrast, the temperature above the inner surface of the ceiling board differed between the night- and day-time. In the day-time, the temperature considerably increased with the height and reached the maximum at the inner surface of the roof tile; the temperature difference between the attic and inner roof surface was particularly large, owing to the solar radiation heating. The temperature of the outer surface of the roof tile was lower than that of the inner surface, probably owing to the transient evaporation cooling upon the showers and heat storage of the tile. On the other hand, the temperature above the ceiling during the night-time exhibited a considerable decrease along the height direction, probably owing to the nocturnal radiative cooling. Nevertheless, considering the higher room air temperature than the outer roof surface temperature by approximately 4 °C during the night-time, the nocturnal cooling was not sufficient to exceed the heat storage to cool the room air, and thus was not an effective passive cooling method for this house.

In the case NV-R, the temperature gradient of the room air was smaller than in case NV, which implies that the reduction in solar heat gain at the roof could attenuate the indoor temperature variation. The temperatures of both sides of the ceiling surface were slightly lower than indoor air temperature during both night-time and day-time. Similar trends were observed in the other three cases with retrofitting.

In the three cases with the ceiling insulation (NV-R-C and NV-R-C-F), we can confirm the effect of the insulation by the equivalent temperature of the inner ceiling surface in the day-time and night-time.

3.5. Effect of the roof shading on the thermal load

Fig. 14 shows the temperature differences between the roof surface and outdoor air, $\Delta T_r = (T_{rst} - T_o)$, during the day-time after every 15 min under various solar radiation conditions. The temperature differences for the neighbouring roof without roof cover are also presented for comparison. The data were classified by two weather conditions, fair and raining days. The raining day was identified by referring to the time-series solar radiation data in Fig. 9a. An abrupt decrease in the solar radiation indicated rainfall in the considered period. The temperature differences between the roof surface and outdoor air for a fair day without the roof cover exhibited a positive correlation with solar radiation, as expected, and reached approximately 20 °C at solar radiation of 900 W/m². In contrast, the increase in the temperature differences between the roof surface and outdoor air on a fair day with the roof cover was marginal (in the range of -2 to 4 °C). This suggests that the roof shading considerably reduced the surface heating by solar radiation. For the rainy days, the plot scatters were larger than those for the fair days. The large scatter in the case without the cover at a small solar radiation might be caused by the transient decrease in solar radiation due to the showers. The positive effect of the roof cover for the reduction in heat gain into the building is consistent with the studies by Zingre et al. [21] and Omar et al. [22] on shading by a double-skin roof.

To quantify the convective heat, which contributed to the increases in air temperatures of the roof attic and bedroom, the convective heat fluxes Q_h [42] were estimated,

$$Q_h = h_c(T_s - T_a), \quad (2)$$

where h_c is the convective heat transfer coefficient, T_s is the surface temperature, and T_a is the air temperature. Convective heat fluxes for the attic was calculated based on the temperature difference between the inner surface of the roof tile and air temperature in the attic. Convective heat fluxes between the ceiling and room was calculated by using the temperature difference between bottom surface of the ceiling and air temperature in the room. Fig. 15 illustrates the convective heat fluxes between the roof tiles and attic air and between the ceiling board and master bedroom air. Convective heat transfer coefficient of the roof tiles was set to 3.87 W/m²·K (tilted surface), and that of the ceiling was set to 4.04 W/m²·K (horizontal surface [42]).

Fig. 16 shows the time variation in estimated convective heat fluxes for four cases. In the case NV, the maximum convective heat fluxes from the roof tiles for the first three days was high (50–65 W/m²) at noon. On the fourth and fifth days, owing to the rain, convective heat fluxes from the roof tiles was substantially reduced. In the case NV-R, the maximum convective heat fluxes from the roof tiles at noon was considerably reduced to approximately 15–25

W/m². Thus, the roof cover reduced the thermal load through convection by 60–70%. The data for NV-R-C and NV-R-C-W do not considerably differ from those for NV-R.

For the master bedroom, the daily maximum convective heat fluxes in case NV was approximately 18–22 W/m² (at 13:00 with a time lag of 1 h compared to convective heat fluxes of the attic). In case NV-R, convective heat fluxes was considerably reduced to 1–4 W/m². Fig. 17 shows the heat fluxes over 24 h on a clear day (first day of NV and NV-R). The pattern of the graph is the same as the finding by Singh et al. [43] on roof surface in summer in India with a peak heat flux of 68.1 W/m². Furthermore, when the heat insulation slab was added to the ceiling, the maximum convective heat fluxes in the room was reduced to 2 W/m². In contrast, the minimum convective heat fluxes in the room was measured at night-time when indoor air temperature was higher than bottom surface temperature of the ceiling. Convective heat fluxes increased from -6 W/m² in NV-R to -3 W/m² in NV-R-C. Similar to attenuation of the roof heating in day-time, the insulation of the ceiling attenuated the nocturnal radiation cooling from the rooftop at night-time.

As the solar radiation values differed between the days and cases (Fig. 8a) owing to precipitation, fair days with similar daily total solar radiation of 14.7–16.1 MJ/day were considered for comparison of the scatter plots of Q_h versus SR for the four cases (Fig. 18). The graph shows a significant reduction in convective heat fluxes in the attic with the roof cover. The maximum convective heat fluxes reduced from 70 to approximately 10 W/m² (Fig. 18a) in the attic, and from 25 to approximately 3 W/m² (Fig. 18b) in the room. However, during the night-time after the sunset at 19:00, even though solar radiation was zero, the heat absorbed in the roof tiles during the day acted as a heat source and contributed to the increase in attic air temperature through the convectively transported heat. For better comparison, particularly at night-time, a similar scatter plot of Q_h against the equivalent outdoor temperature (T_{eq}) is shown in Fig. 18c for the attic and Fig. 18d for the room. T_{eq} is expressed by T_o , SR , and solar absorptivity (a) of the roof tiles [44] (Eq. 3). The absorptivity of the orange light of the roof tiles was set to 0.6 [45].

$$T_{eq} = T_o + a(SR/h). \quad (3)$$

Fig. 18c,d shows the effects of solar radiation and outdoor air temperature for a whole day, including night-time. The effect of the roof cover on the reduction in convective heat fluxes in the attic was emphasised when equivalent outdoor

temperature was above 30 °C (Fig. 18c), and 25 °C (Fig. 18d) in the room. When equivalent outdoor temperature was below 25 °C, the room temperature was higher than outdoor, which led to a negative convective heat flux.

To further analyse the effect of the roof retrofitting on the indoor thermal environment, the temperature difference between the indoor and outdoor, $\Delta T = T_i - T_o$, was plotted against T_{eq} . Fig. 19 shows the negative correlation between equivalent outdoor temperature and the temperature difference between the indoor and outdoor. Even though the plots of the different cases were scattered and overlapped, the temperature difference between the indoor and outdoor were observed by comparing the four regression lines. The temperature difference between the indoor and outdoor, estimated based on the regression line, had the highest value in case NV when equivalent outdoor temperature was higher than 30 °C, while the lowest value was observed for NV-R-C-F, indicating that the three types of retrofitting and ceiling fan effectively reduced the room air temperature during the hot day-time with a large solar radiation. During the night-time at equivalent outdoor temperature below 26 °C, all cases exhibited large scatters. The temperature difference between the indoor and outdoor had the lowest value in case NV, which suggests that the influences of the retrofitting and ceiling fan on indoor air temperature were marginal.

3.6. Comparison of the indoor comfort temperatures by using adaptive comfort standards

Adaptive thermal comfort standards were used to evaluate the thermal measurement data. According to the various adaptive comfort standards, the acceptable indoor comfort temperature based on operative temperature for a naturally ventilated space can be predicted by using outdoor air temperature. The different standards use slightly different equations for the prediction of the comfort temperature. The American Society of Heating, Refrigerating, and Air-Conditioning Engineers (ASHRAE) Standard 55-2017 [46] defines the acceptable thermal environment for occupant-controlled naturally conditioned spaces based on a neutral value of operative temperature between the 80% upper and lower acceptability limits of operative temperature in the space,

$$T_{comf-op} = 0.31 T_{mm} + 17.8, \quad (4)$$

where $T_{comf-op}$ is the indoor neutral T_{op} (°C), and T_{mm} is the monthly mean outdoor air temperature (°C). In contrast, the European Standard (EN) 16798-1 [47] is based on a different equation for the calculation of acceptable indoor temperatures for buildings without mechanical cooling systems,

$$T_{\text{comf-op}} = 0.33T_{\text{rm}} + 18.8, \quad (5)$$

where T_{rm} is the running mean outdoor air temperature (°C). Toe and Kubota [48] proposed an adaptive thermal comfort equation (ACE) for naturally ventilated buildings in hot-humid climates by using the ASHRAE RP-884 database,

$$T_{\text{comf-op}} = 0.57T_{\text{dm}} + 13.8, \quad (6)$$

where T_{dm} is the daily mean outdoor air temperature (°C). Table 6 summarises the mean measured operative temperature, mean calculated operative temperature, and indoor neutral operative temperature values obtained according to ASHRAE Standard 55-2017, EN 16798-1, and the adaptive thermal comfort equation for the hot-humid climate for all cases.

In Fig. 20, the outdoor air temperature and operative temperature values in all cases are plotted against the three comfortable temperatures predicted by the standards. In the case NV (Fig. 20a), operative temperature generally did not comply with ASHRAE Standard 55-2017 and EN 16798-1. However, for 38% (26% at night and 12% of day) of the period, operative temperature in case NV was below the acceptable comfortable indoor temperature predicted by the adaptive thermal comfort equation for a hot-humid climate.

In NV-R (Fig. 20b), the values also did not comply with ASHRAE Standard 55-2017 and EN 16798-1. However, the compliance percentage was increased to 48% with respect to the hot-humid-climate adaptive thermal comfort equation. During the day-time, the percentage increased by 2% (to 14%), while during the night-time by 8%. Thus, the roof cover improved the thermal performance of the room by 10% compared to the case NV.

Fig. 20c shows the results after the introduction of the heat insulation slab on the ceiling. For 39% of the period, operative temperature in case NV-R-C was below the acceptable comfortable indoor temperature predicted by the adaptive thermal comfort equation for a hot-humid climate. The compliance during the day-time was maintained at 14%, but during the night-time, it decreased from 34% to 25%. The low performance of the heat insulation slab in the attic is not consistent with the findings by Kachkouch et al. [29], possibly as the earlier installation of the roof cover before the installation of the heat insulation slab has blocked most of the convective heat from the roof to the ceiling. The installation of the heat insulation slab above the ceiling did not block the heat from entering the roof during the day but prevented heat release through the ceiling at night.

In NV-R-C-F (Fig. 20d), the compliance percentage was very high for 92% of the period, operative temperature was within the acceptable comfortable indoor temperatures predicted by adaptive thermal comfort equation for a hot–humid climate and 13% by EN 16798-1. Notably, the compliance reached 100% of the adaptive thermal comfort equation for a hot–humid climate during the night-time. The increase in indoor thermal comfort temperature by the ceiling fan is consistent with the study by Nicol et al. [49]. In his review on the effect of wind on the thermal comfort, Rijal [50] has concluded that the increased wind velocity increases the comfort temperature, particularly in hot and humid climate regions. Table 6 summarise the compliance of operative temperature in the room to ASHRAE Standard 55-2017, EN 16798-1 and ACE hot-humid for the four cases of study.

4. Conclusions

The objective of this study was to evaluate the efficiencies of the various retrofitting methods for the improvement in the indoor thermal environment of the terrace house, particularly by using the roof cover under the hot and humid climate.

- Complete ventilation was not sufficient to achieve the predicted comfortable indoor temperatures. However, with respect to the adaptive thermal comfort equation for a hot–humid climate, for 38% of the period, compliance of T_{op} was achieved in case NV.
- The roof cover reduced air temperature in attic by approximately 1.4 °C on average for a whole day and by up to 3.5 °C in the day-time. In the room, the reduction was 0.8 °C on average for a whole day, but there was no reduction during the day-time.
- The roof cover reduced the convective heat fluxes in the attic and room by 70–80% and 88%, respectively.
- The building retrofitting with the roof cover increased the compliance with the ACE for a hot–humid climate by 10%.
- The heat insulation above the ceiling was not effective for the blockage of heat from the roof. It did not improve compliance (maintained at 14%) during day-time. During night-time, the compliance was further reduced from 34 to 25%. The heat insulation slab trapped the heat in the room and prevented its escape from the roof through the ceiling.

- The active cooling with the ceiling fan effectively achieved the required comfortable indoor temperature under the hot–humid climate, particularly during the night-time.

This study shows that the roof cover can effectively provide thermal comfort in residential buildings in Malaysia having a hot–humid climate. The low-cost installation (3.6 USD/m² including materials and labour) of the HDPE net as the roof cover (compared to 167–310 USD/m² for the PV installation) is affordable for most house owners in Malaysia. The proposed zero-energy-consumption low-cost method is suitable for landed houses in the Southeast Asian regions with hot–humid climates. Furthermore, for remote areas without electricity, the roof cover can provide an effective means of passive cooling. Further studies can be conducted on the application of the roof cover in traditional houses in Southeast Asia.

The limitation of this study was the durability of the material used as the roof cover. The HDPE net will deteriorate gradually with time because it was originally designed for temporal use in agriculture. It is also weak against strong-wind, which should be also noted, although strong weather events such as typhoons and hurricanes rarely occur in the tropics. Therefore, to widely implement this roof cover system, it is necessary to select appropriate materials that can withstand long-term outdoor use and to develop a fixing details that can be easily attached and detached in strong winds. Furthermore, no precipitation data were collected in this study. Thus, it is strongly recommended to include a precipitation study in any future research related to thermal comfort.

Funding

This research was supported by the Malaysian Ministry of Higher Education (MOHE) under the Research University Grant [grant number 18H00].

References

- [1] United Nations, Energy statistics pocketbook2018. <https://unstats.un.org/unsd/energy/pocket/2018/2018pb-web.pdf> (accessed March 12, 2019).
- [2] International Energy Agency, The future of cooling2018. <https://doi:10.1787/9789264301993-en>.
- [3] Suruhan Tenaga Malaysia, National energy balance 2016, 2016. <http://meih.st.gov.my/documents/10620/9a9314a1-cf11-4640-a9de-3b31f336a416>.
- [4] Y. Zhou, C. Lork, W.T. Li, C. Yuen, Y.M. Keow, Benchmarking air-conditioning energy performance of residential rooms based on regression and clustering techniques, Appl. Energy 253 (2019) 113548. <https://doi:10.1016/j.apenergy.2019.113548>.

- [5] A. Dominguez, J. Kleissl, J.C. Luvall, Effects of solar photovoltaic panels on roof heat transfer, *Solar Energy* 85 (2011) 2244-2255. <https://doi.org/10.1016/j.solener.2011.06.010>.
- [6] T. Chenvidhya, M. Seapan, P. Parinya, B. Wiengmoon, D. Chenvidhya, R. Songprakorp, C. Limsakul, Y. Sangpongsanont, N. Tannil, Investigation of power values of PV rooftop systems based on heat gain reduction, in: 8th Reliab. Photovolt. Cells, Modul. Components Syst. Conf., SPIE - The International Society for Optical Engineering, 2015.
- [7] T. Terlouw, T. AlSkaif, C. Bauer, W. van Sark, Optimal energy management in all-electric residential energy systems with heat and electricity storage, *Appl. Energy* 254 (2019) 113580. <https://doi.org/10.1016/j.apenergy.2019.113580>.
- [8] T. Kubota, D.T.H. Chyee, S. Ahmad, The effects of night ventilation technique on indoor thermal environment for residential buildings in hot-humid climate of Malaysia, *Energ. Buildings* 41 (2009) 829-839. <https://doi.org/10.1016/j.enbuild.2009.03.008>.
- [9] M. Santamouris, A. Sfakianaki, K. Pavlou, On the efficiency of night ventilation techniques applied to residential buildings, *Energ. Buildings* 42 (2010) 1309-1313. <https://doi.org/10.1016/j.enbuild.2010.02.024>.
- [10] K. Imessad, L. Derradji, N.A. Messaoudene, F. Mokhtari, A. Chenak, R. Kharchi, Impact of passive cooling techniques on energy demand for residential buildings in a Mediterranean climate, *Renew. Energy* 71 (2014) 589-597. <https://doi.org/10.1016/j.renene.2014.06.005>.
- [11] V. Pérez-Andreu, C. Aparicio-Fernández, A. Martínez-Ibernón, J.-L. Vivancos, Impact of climate change on heating and cooling energy demand in a residential building in a Mediterranean climate, *Energy* 165 (2018) 63-74. <https://doi.org/10.1016/j.energy.2018.09.015>.
- [12] Z. Ma, P. Cooper, D. Daly, L. Ledo, Existing building retrofits: Methodology and state-of-the-art, *Energ. Buildings* 55 (2012) 889-902. <https://doi.org/10.1016/j.enbuild.2012.08.018>.
- [13] M. Rabani, H.B. Madessa, N. Nord, A state-of-art review of retrofit interventions in buildings towards nearly zero energy level, *Energy Procedia* 134 (2017) 317-326. <https://doi.org/10.1016/j.egypro.2017.09.534>.
- [14] W.T. Li, S.R. Gubba, W. Tushar, C. Yuen, N.U. Hassan, H.V. Poor, K.L. Wood, C.K. Wen, Data Driven Electricity Management for Residential Air Conditioning Systems: An Experimental Approach, *IEEE Trans. Emerg. Topics Comput.* 2017. <https://doi.org/10.1109/TETC.2017.2655362>.
- [15] N. Wai Tuck, S.A. Zaki, A. Hagishima, H.B. Rijal, M.A. Zakaria, F. Yakub, Effectiveness of free running passive cooling strategies for indoor thermal environments: example from a two-storey corner terrace house in Malaysia, *Build. Environ.* 160 (2019) 106214. <https://doi.org/10.1016/j.buildenv.2019.106214>
- [16] I. Oropeza-Perez, P.A. Østergaard, Active and passive cooling methods for dwellings: A review, *Renew. Sustain. Energy Rev.* 82 (2018) 531-544. <https://doi.org/10.1016/j.rser.2017.09.059>.
- [17] L. Lan, W. Tushar, K. Otto, C. Yuen, K.L. Wood, Thermal comfort improvement of naturally ventilated patient wards in Singapore, *Energy Build.* 154 (2017) 499-512. <https://doi.org/10.1016/j.enbuild.2017.07.080>.
- [18] D.H.C. Toe, T. Kubota, Comparative assessment of vernacular passive cooling techniques for improving indoor thermal comfort of modern terraced houses in hot-humid climate of Malaysia, *Solar Energy* 114 (2015) 229-258. <https://doi.org/10.1016/j.solener.2015.01.035>.
- [19] K.M. Al-Obaidi, M. Ismail, A.M. Abdul Rahman, Passive cooling techniques through reflective and radiative roofs in tropical houses in Southeast Asia: A literature review, *Front. Archit. Res.* 3 (2014) 283-297. <https://doi.org/10.1016/j.foar.2014.06.002>.
- [20] M. Abuseif, Z. Gou, A review of roofing methods: construction features, heat reduction, payback period and climatic responsiveness, *Energies* 11 (2018) 3196. <https://doi.org/10.3390/en11113196>.
- [21] K.T. Zingre, M. Pun, S. Khian, W. Boo, T. Toh, I. Yen, L. Lee, Modelling of cool roof performance for double-skin roofs in tropical climate, *Energy* 82 (2015) 813-826. <https://doi.org/10.1016/j.energy.2015.01.092>.
- [22] I. Omar, J. Virgone, D. David, O. Le Corre, Energy saving potential with a double-skin roof ventilated by natural convection in Djibouti, *Energy Procedia* 140 (2017) 361-373.

<https://doi:10.1016/j.egypro.2017.11.149>.

- [23] K.T. Zingre, E. Yang, M. Pun Wan, Dynamic thermal performance of inclined double-skin roof: modeling and experimental investigation, *Energy* 133 (2017) 900-912. <https://doi:10.1016/j.energy.2017.05.181>.
- [24] G. Osuma-Pinto, G. Ordóñez-Plata, Measuring factors influencing performance of rooftop PV panels in warm tropical climates, *Solar Energy* 185 (2019) 112-123. <https://doi:10.1016/j.solener.2019.04.053>.
- [25] F. Muhammad-sukki, R. Ramirez-iniguez, S.H. Abu-bakar, S.G. Mcmeekin, B.G. Stewart, An evaluation of the installation of solar photovoltaic in residential houses in Malaysia : past, present, and future, *Energy Policy* 39 (2011) 7975-7987. <https://doi:10.1016/j.enpol.2011.09.052>.
- [26] L. Lan, K.L. Wood, C. Yuen, A holistic design approach for residential net-zero energy buildings: A case study in Singapore, *Sustain. Cities Soc.* 50 (2019) 101672. <https://doi:10.1016/j.scs.2019.101672>.
- [27] S.E.D.A. Malaysia, Go solar and save on your electricity bill2019. <http://www.seda.gov.my/2019/05/go-solar-and-save-on-your-electricity-bill/> (accessed June 23, 2019).
- [28] Department of Statistics Malaysia Official Portal, 2017. https://www.dosm.gov.my/v1/index.php?r=column/cthemebByCat&cat=120&bul_id=RUZ5REwveU1ra1hGL21JWVlPRmU2Zz09&menu_id=amVoWU54UTl0a21NWmdhMjFMMWcyZz09 (accessed August 15, 2019).
- [29] S. Kachkouch, F. Ait-nouh, B. Benhamou, K. Limam, Experimental assessment of thermal performance of three passive cooling techniques for roofs in a semi-arid climate, *Energy Build.* 164 (2018) 153-164. <https://doi:10.1016/j.enbuild.2018.01.008>.
- [30] A. Mistriotis, S. Hemming, D. Waaijenberg, Plastic nets in agriculture: a general review of types and applications, *Appl. Eng. Agric.* 24 (2008) 799-808.
- [31] P. Soni, V.M. Salokhe, H.J. Tantau, Effect of screen mesh size on vertical temperature distribution in naturally ventilated tropical greenhouses, *Biosyst. Eng.* 92 (2005) 496-482. <https://doi:10.1016/j.biosystemseng.2005.08.005>.
- [32] K.S. Teh, D.W. Yarbrough, C.H. Lim, E. Salleh, Reflective insulation for energy conservation in south east Asia, *IOP Conference Series: Earth and Environmental Science* 63 (2017) 012047. <https://doi:10.1088/1755-1315/63/1/012047>.
- [33] Jabatan Perangkaan Malaysia, Ciri-ciri tempat kediaman 2010, 2012. <https://www.dosm.gov.my>.
- [34] Residential, commercial and industrial properties status report 2018, Pusat Maklumat Harta Tanah Negara, Jabatan Penilaian dan Perkhidmatan Harta, Kementerian Kewangan Malaysia, Pusat Maklumat Harta Tanah Negara, Jabatan Penilaian dan Perkhidmatan Harta, Kementerian Kewangan Malaysia, Malaysia, 2018.
- [35] H.A. Swarno, S.A. Zaki, Y. Yusup, M.S.M. Ali, N.H. Ahmad, Observation of diurnal variation of urban microclimate in Kuala Lumpur, Malaysia, *Chem. Eng. Trans.* 56 (2017) 523-528. <https://doi:10.3303/CET1756088>.
- [36] W. Khalid, S.A. Zaki, H.B. Rijal, F. Yakub, Investigation of comfort temperature and thermal adaptation for patients and visitors in Malaysian hospitals, *Energy Build.* 183 (2019) 484-499. <https://doi:10.1016/j.enbuild.2018.11.019>.
- [37] UAC Berhad, UCO-Supeflex2019. <http://uac.com.my/wp-content/uploads/2017/08/UCO-Supeflex.pdf> (accessed June 6, 2019).
- [38] Department of Standards Malaysia, Malaysian Standard energy for residential buildings - Code of practice, Malaysia, 2017.
- [39] R. Saidur, M. Hasanuzzaman, M.M. Hasan, H.H. Masjuki, Overall thermal transfer value of residential buildings in Malaysia, *J. Appl. Sci.* 9 (2009) 2130-2136.
- [40] C. Kabre, A new thermal performance index for dwelling roofs in the warm humid tropics, *Build. Environ.* 45 (2010) 727-738. <https://doi:10.1016/j.buildenv.2009.08.017>.

- [41] P. Bevilacqua, D. Mazzeo, R. Bruno, N. Arcuri, Experimental investigation of the thermal performances of an extensive green roof in the Mediterranean area, *Energy Build.* 122 (2016) 63-79. <https://doi:10.1016/j.enbuild.2016.03.062>.
- [42] EnergyPlus (US Department of Energy), Engineering Reference, EnergyPlus, US Department of Energy, EnergyPlus, US Department of Energy, 2019.
- [43] M.K. Singh, H.B. Rijal, N. Member, N.K. Bansal, The Effect of Cool Roof on Built Environment in Composite and Hot and Dry Climates of India, in: *Soc. Heating, Air-Conditioning Sanit. Eng. Japan (SHASE), Annu. Conf.*, 2016: pp. 73–76.
- [44] K.A. Al-Saud, Measured versus calculated roof peak sol-air temperature in hot-arid regions, *Red* 29 (2009) 95.
- [45] Monier concrete roof tiles 2019. <https://www.monier.com.au/products/concrete-tiles/elabana> (accessed July 6, 2019).
- [46] ANSI/ASHRAE Standard 55-2013: Thermal environmental conditions for human occupancy, American Society of Heating, Refrigerating and Air-Conditioning Engineers, American Society of Heating, Refrigerating and Air-Conditioning Engineers, United States of America, 2013.
- [47] European Committee for Standardization, DS/EN 15251: Indoor environmental input parameters for design and assessment of energy performance of buildings addressing indoor air quality, thermal environment, lighting and acoustics, 2007. <https://doi:10.1520/E2019-03R13>.
- [48] D.H.C. Toe, T. Kubota, Development of an adaptive thermal comfort equation for naturally ventilated buildings in hot-humid climates using ASHRAE RP-884 database, Elsevier, Elsevier, 2013. <https://doi:10.1016/j.foar.2013.06.003>.
- [49] F. Nicol, Adaptive thermal comfort standards in the hot-humid tropics, 2004. <https://doi:10.1016/j.enbuild.2004.01.016>.
- [50] H.B. Rijal, Thermal adaptation outdoors and the effect of wind on thermal comfort, in: S. Kato, K. Hiyama (Eds.), *Vent. Cities Air-Flow Criteria Heal. Comf. Urban Living*, 2012: pp. 33–58. <https://doi:10.1007/978-94-007-2771-7>.

1

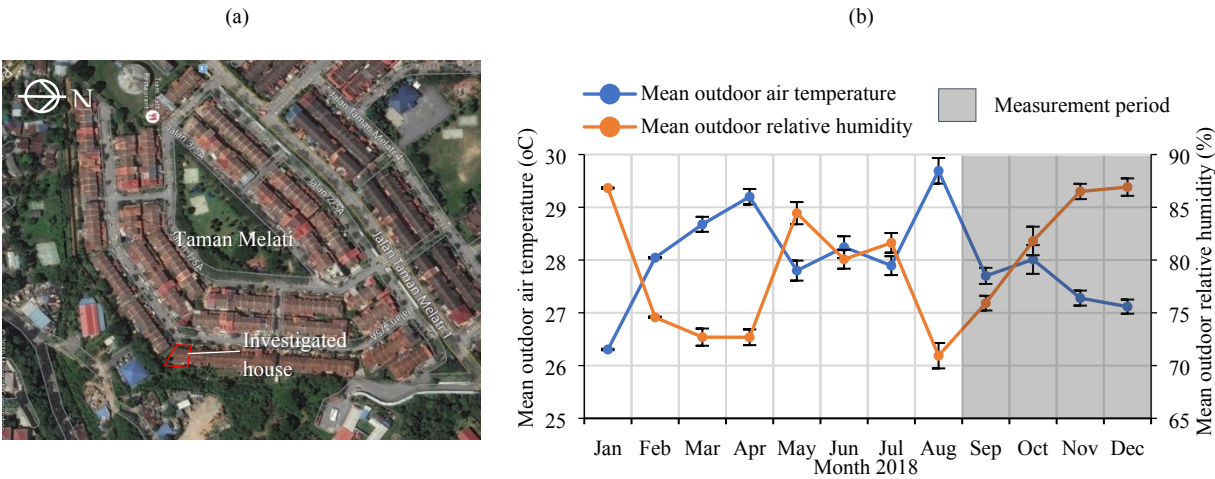
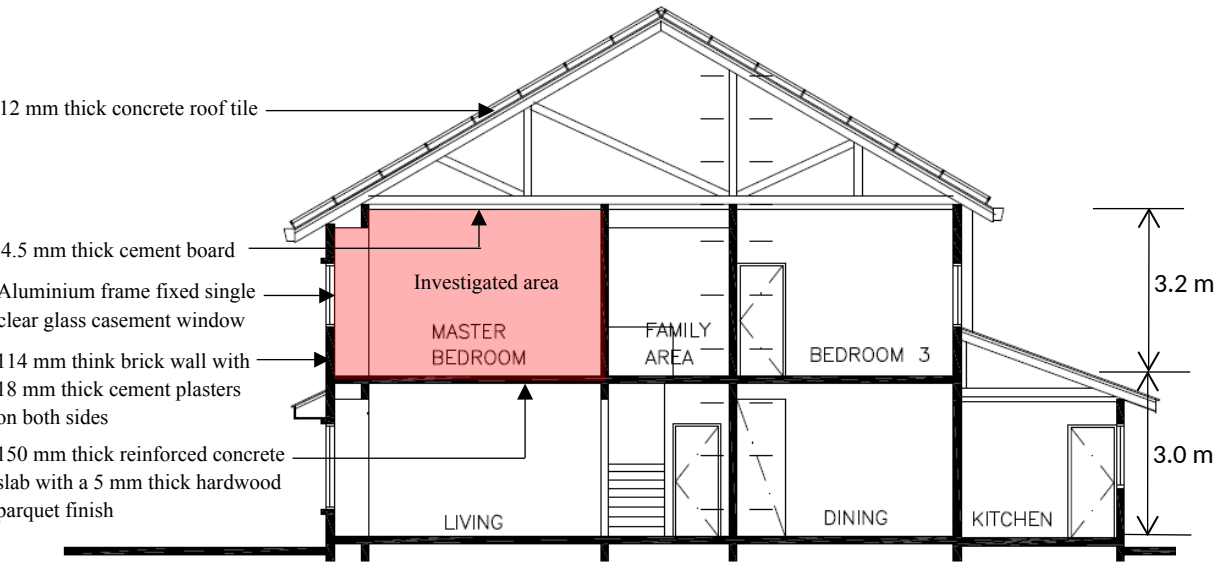


Fig. 1 Location and climate of the investigated house. (a) Map of the region around the investigated house (Google Maps, 2019). (b) Monthly mean outdoor air temperature and *RH* obtained from the weather station at Universiti Teknologi Malaysia in Kuala Lumpur, Malaysia. The error bars indicate the corresponding standard deviations for each month.

5



6

Fig. 2 Section of the investigated house with specification on the building materials.

8

9

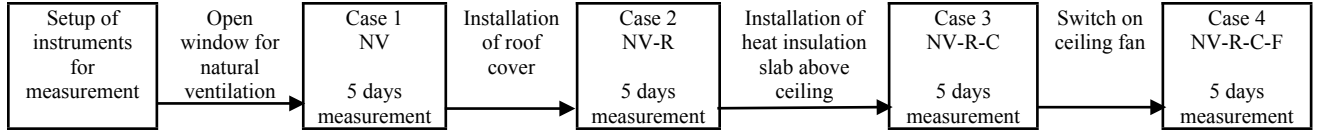


Fig. 3 Flow chart to show the process of study.

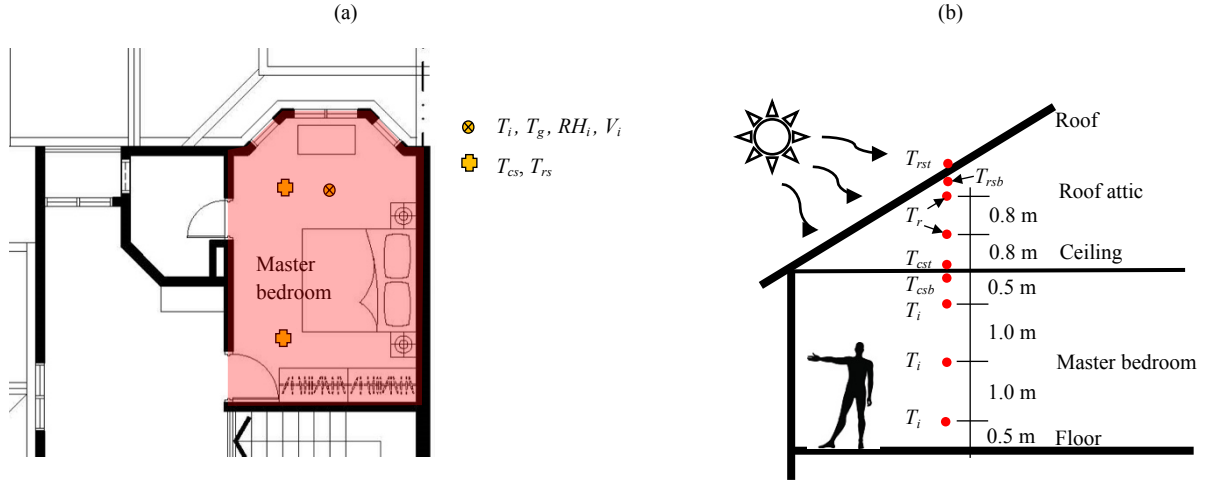


Fig. 4 Setup of the measurement in the master bedroom and attic above the room. (a) Measurement points in the master bedroom. (b) Cross section of the master bedroom and roof, which indicates the measurement points vertically from the floor up to the roof. T_{csb} : ceiling bottom surface temperature, T_{cst} : ceiling top surface temperature, T_r : attic air temperature, T_{rsb} : roof bottom surface temperature, T_{rst} : roof top surface temperature.

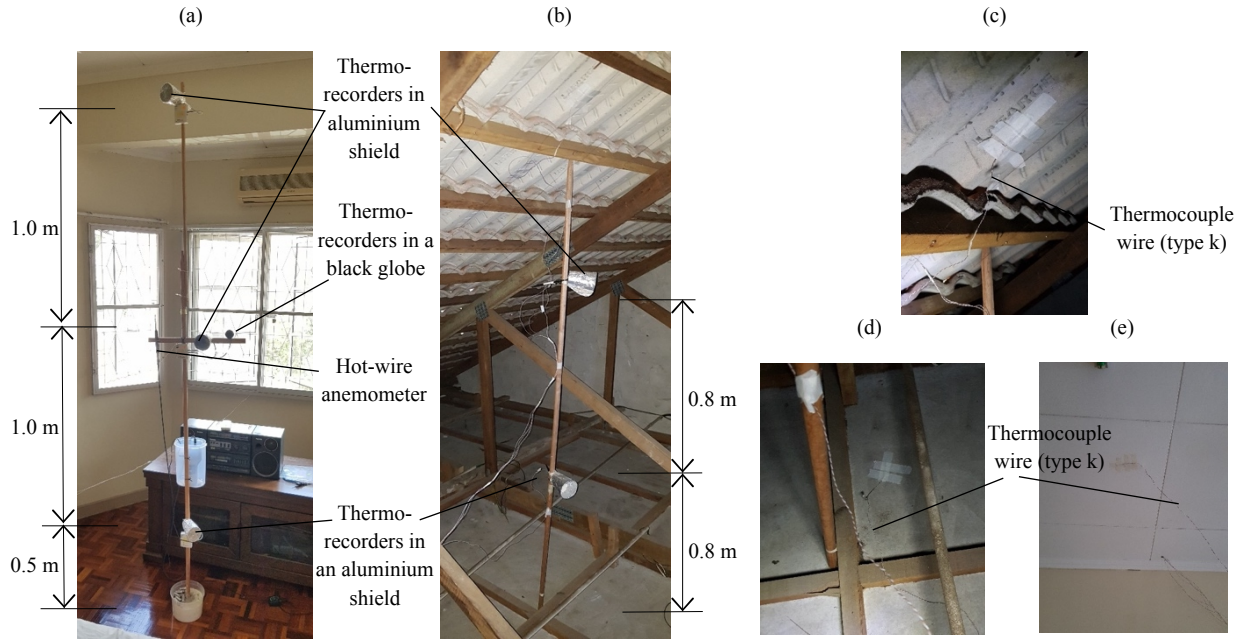


Fig. 5 Setup of the indoor measurement: (a) thermo-recorders, hot-wire anemometer, and thermocouple wire (type k) in the room, (b) at the roof attic, (c) top of the ceiling, (d) bottom of the ceiling, and (e) bottom of the roof tile.

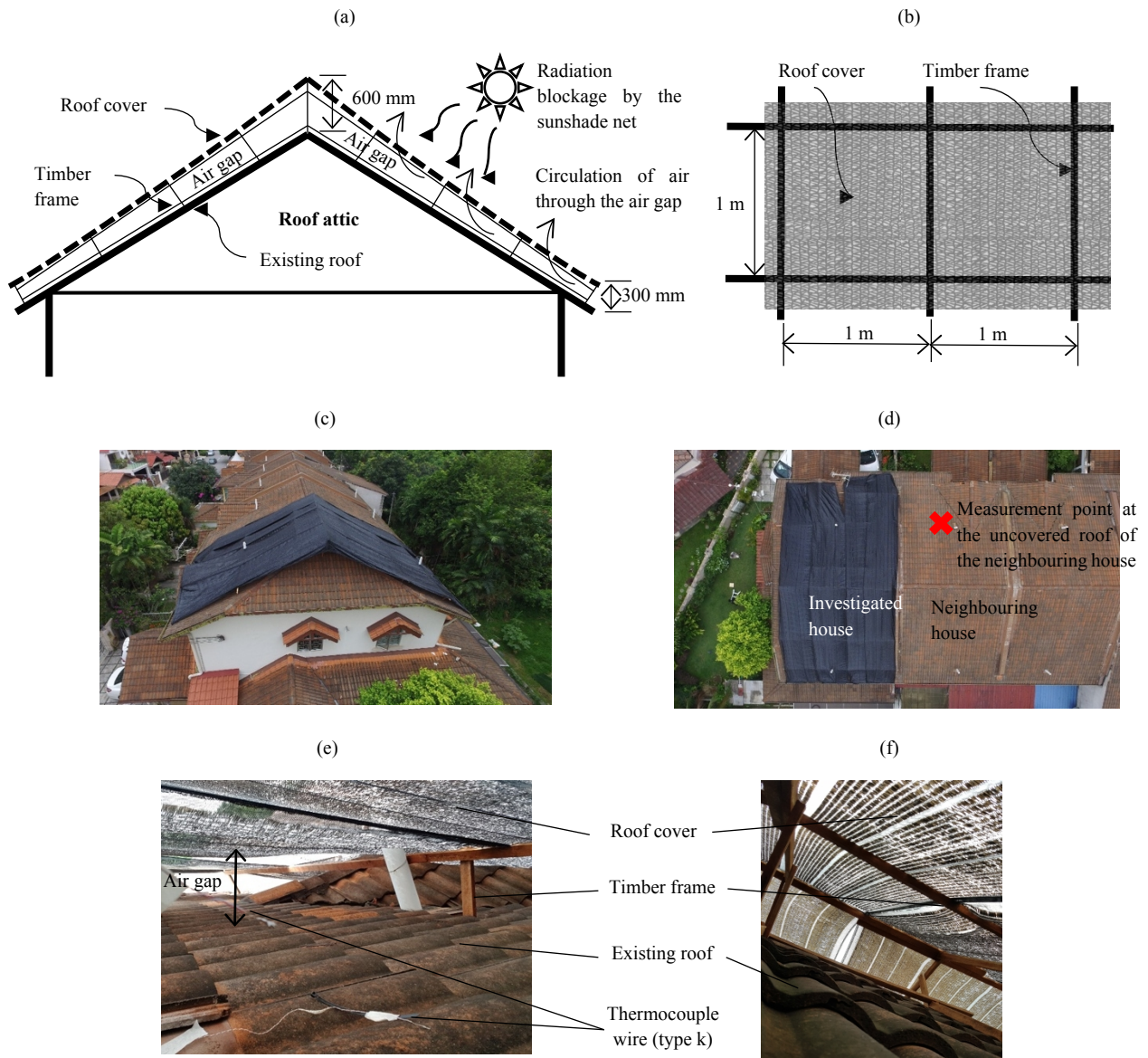


Fig. 6 Installation of the roof cover on the existing roof and measurement setup. (a), (b) Schematics of the installation of the roof cover over the existing roof, (c) existing roof with the HDPE roof cover, (d) measurement point at the uncovered roof tiles of the neighbouring house, and (e), (f) measurement of the temperatures of the top surface of the roof tile and air between the roof cover and roof.

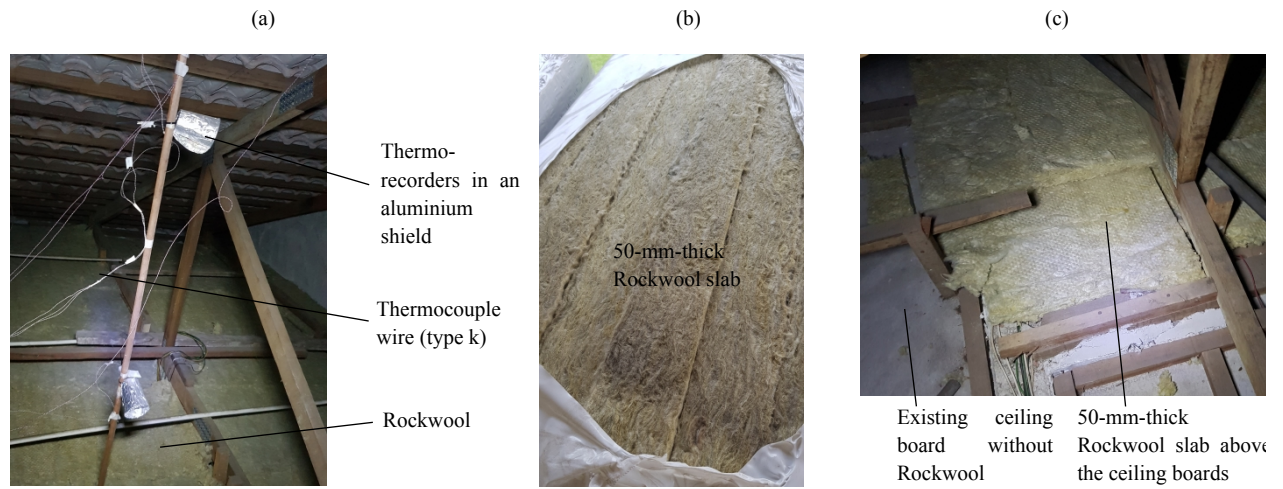


Fig. 7 Installation of the Rockwool slab above the ceiling. (a) Setup of the measurement in the roof, (b) 50-mm-thick Rockwool slab, and (c) Rockwool slab installed above the ceiling boards.

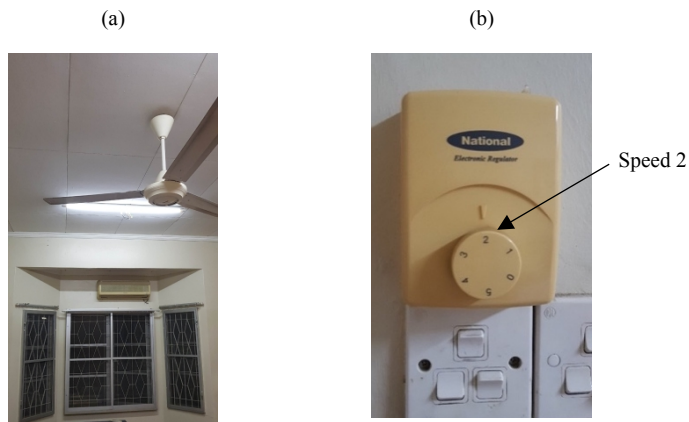


Fig. 8 Case NV-R-C-F. (a) Ceiling fan at the centre of the master bedroom, (b) whose speed was set to 2 (approximately 165 m/min).

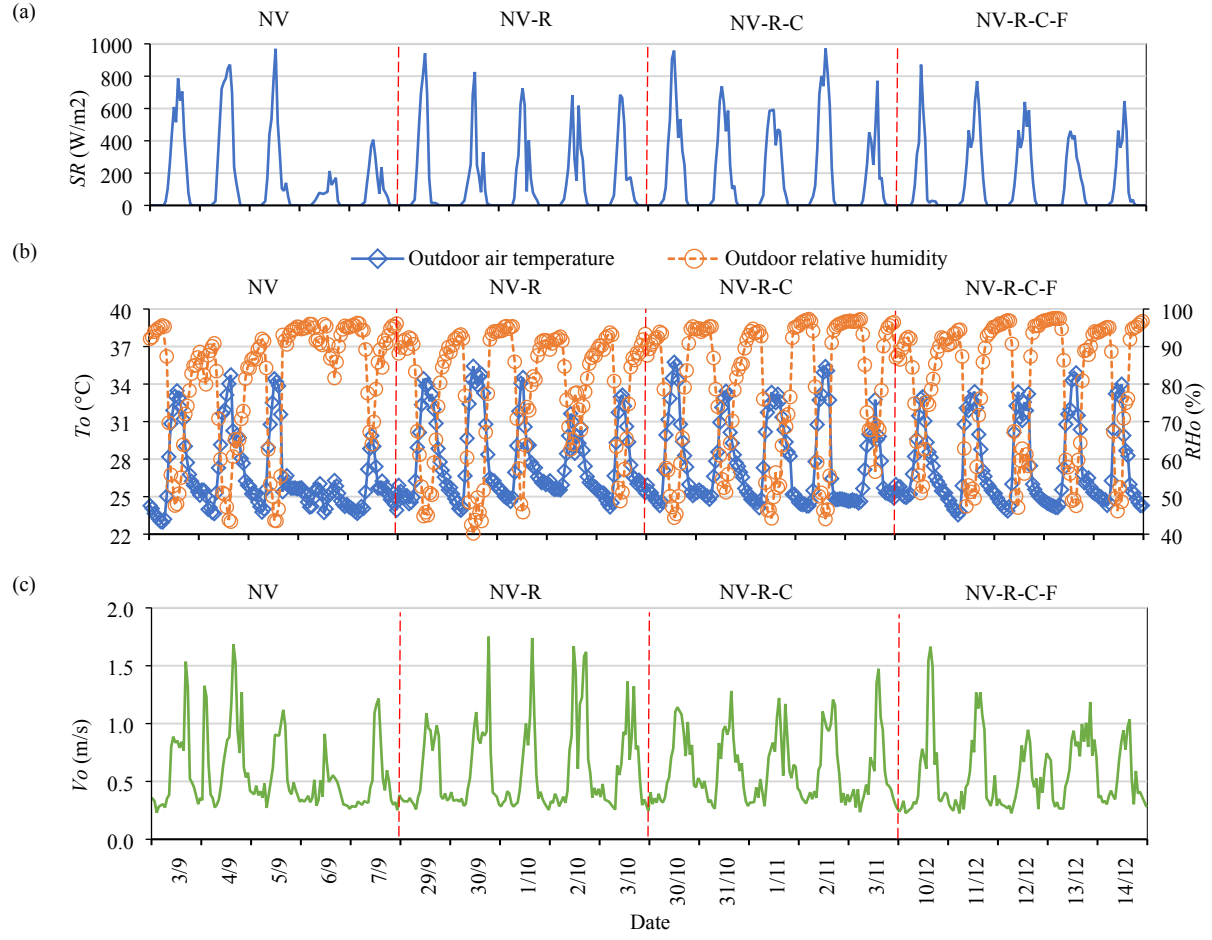
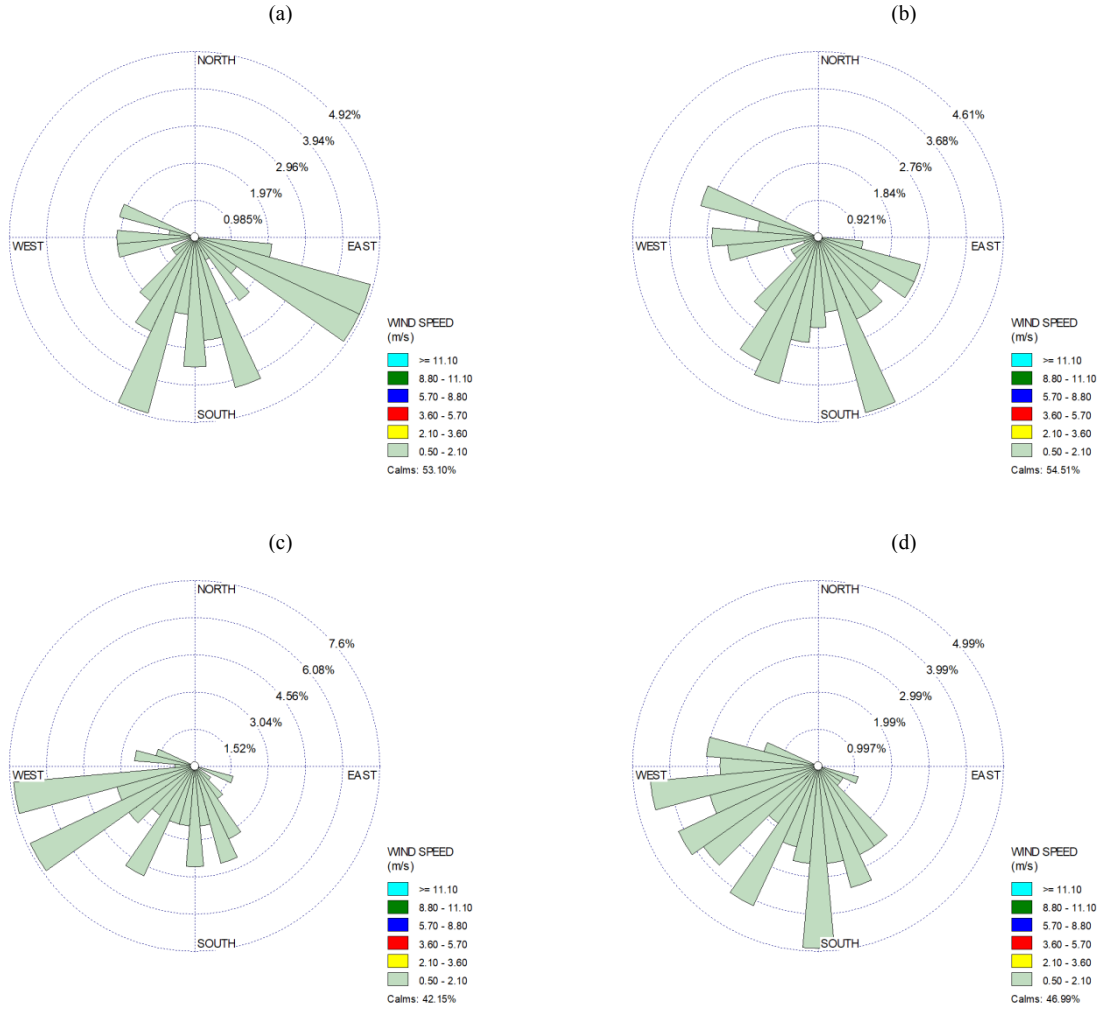


Fig. 9 Outdoor climatic data for the investigated house. (a) SR , (b) T_o and RH , and (c) V_o .



1 Fig. 10 Wind speed and wind direction for (a) NV, (b) NV-R, (c) NV-R-C, and (d) NV-R-C-F.

2

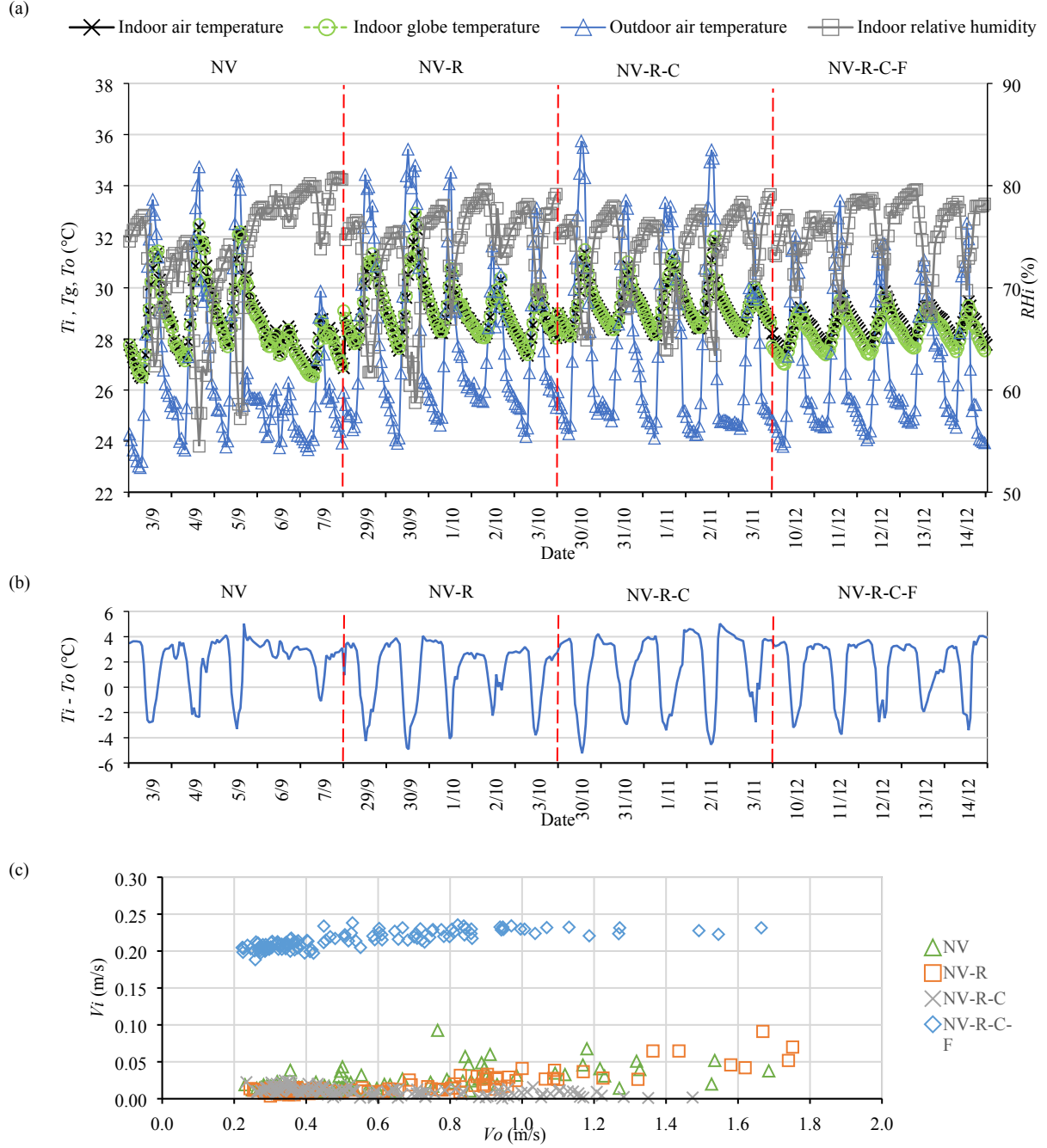


Fig. 11 Indoor climatic data for the master bedroom. (a) T_i , T_g , T_o and RH_i , (b) $T_i - T_o$, and (c) V_i against V_o .

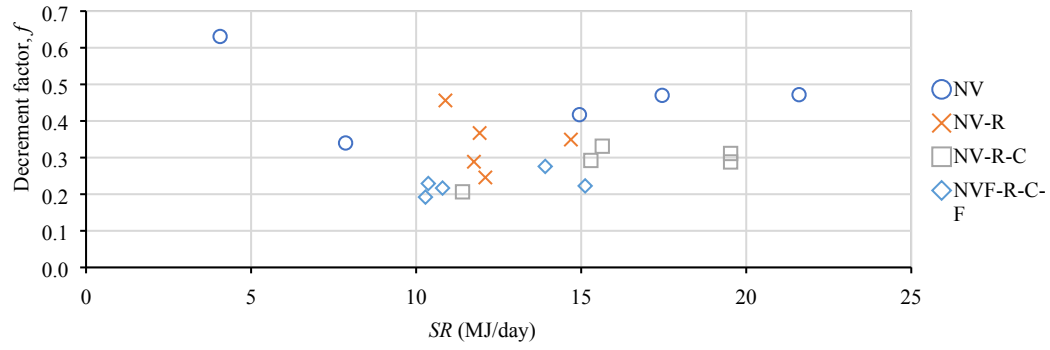


Fig. 12 Relationships between the daily SR and f values (master bedroom).

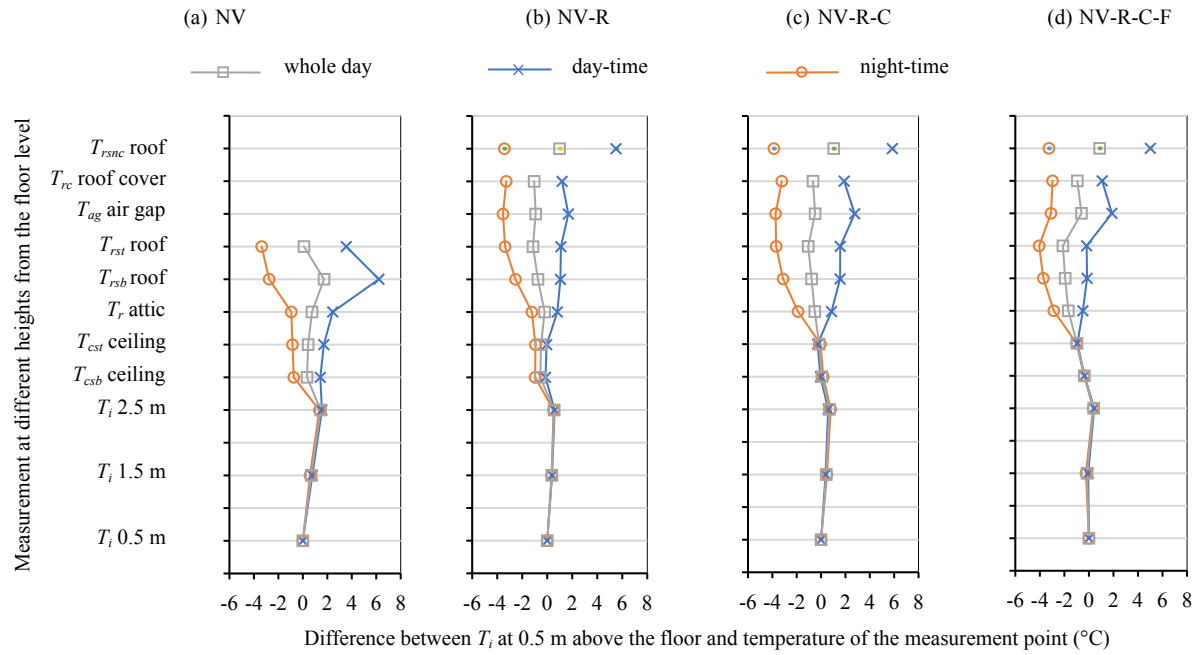


Fig. 13 Differences between T_i at 0.5 m above the floor and temperatures of the measurement points. T_{rsnc} : surface temperature of the roof tile without the roof cover, T_{rc} : surface temperature of the roof cover.

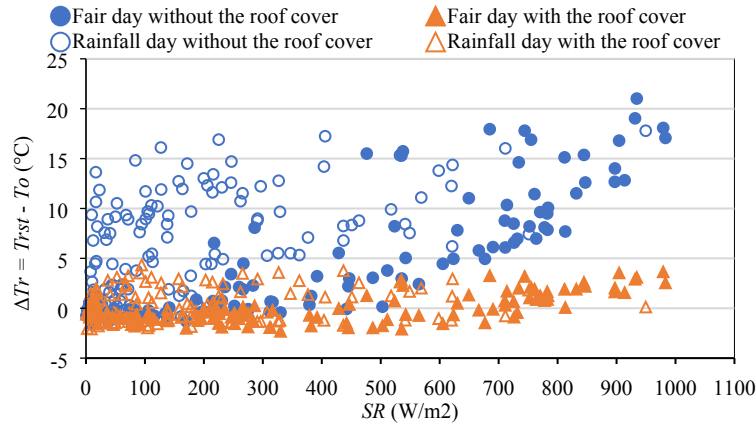


Fig. 14 Temperature difference between the roof top surface and outdoor air in case NV-R, which shows the effect of the roof cover.

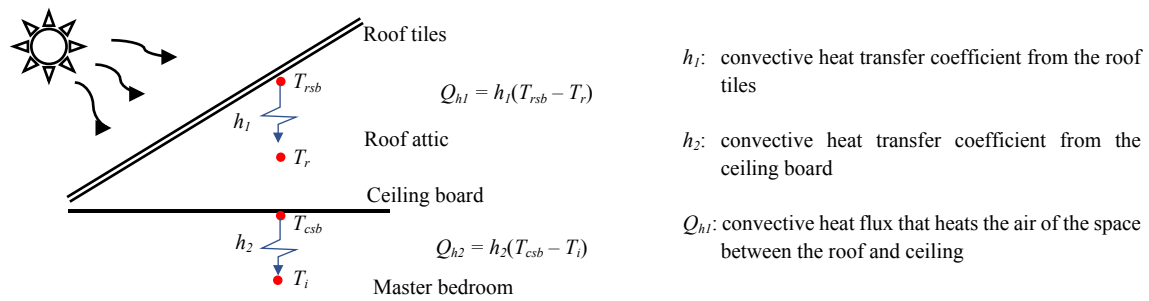


Fig. 15 Convective heat fluxes between the roof tiles and attic air and between the ceiling board and master bedroom air.

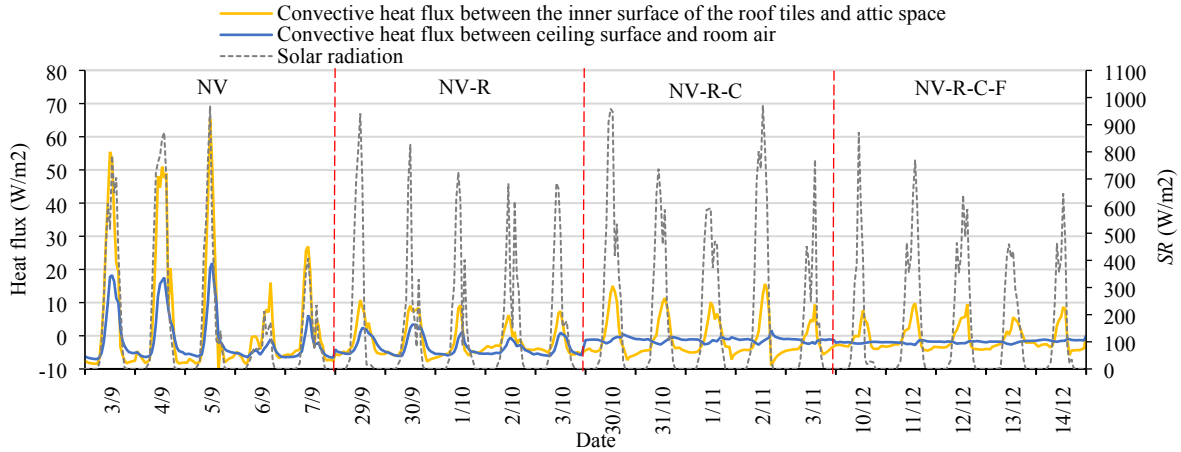


Fig. 16 Convective heat fluxes in the master room and attic.

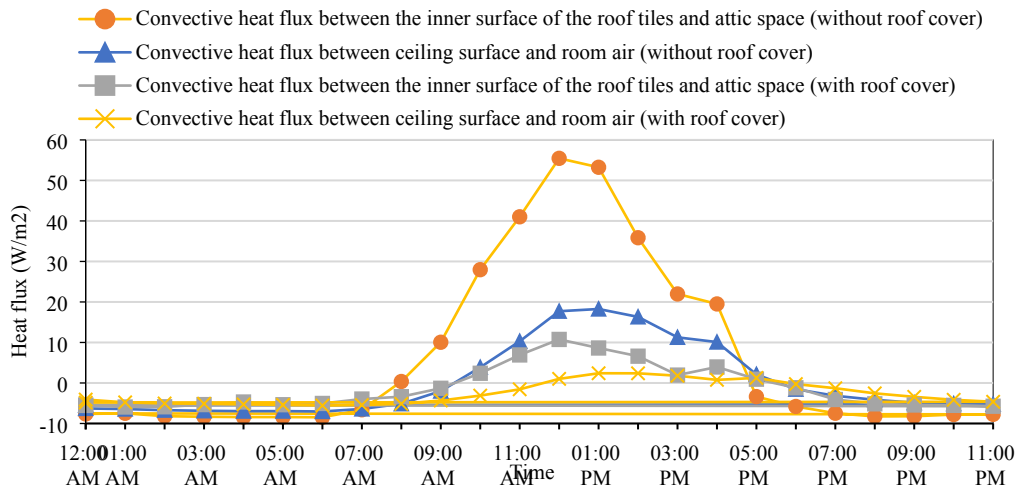


Fig. 17 Comparison of convective heat fluxes in the master room and attic between without roof cover and with roof cover.

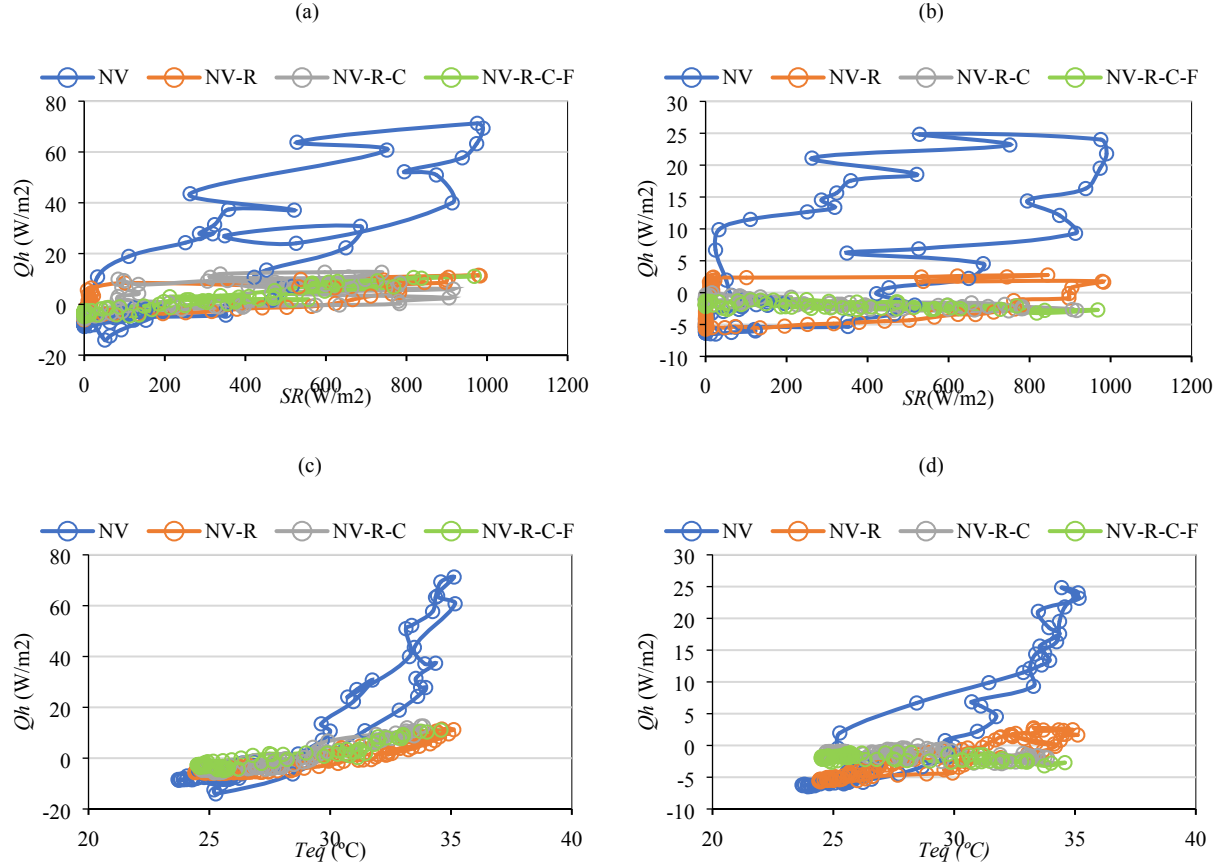


Fig. 18 Q_h values versus SR of the attic (a) and bedroom (b), and Q_h values versus T_{eq} of the attic (c) and bedroom (d), respectively.

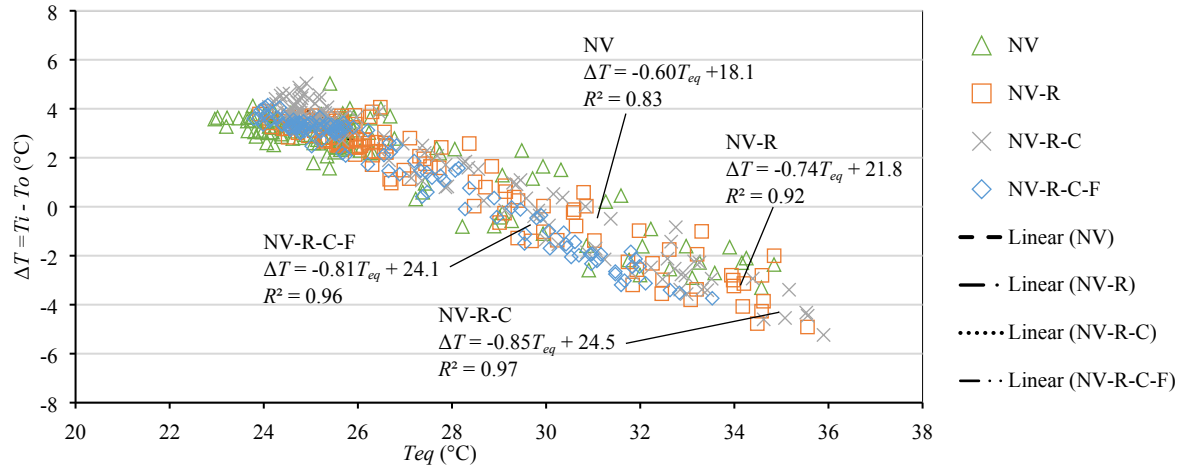
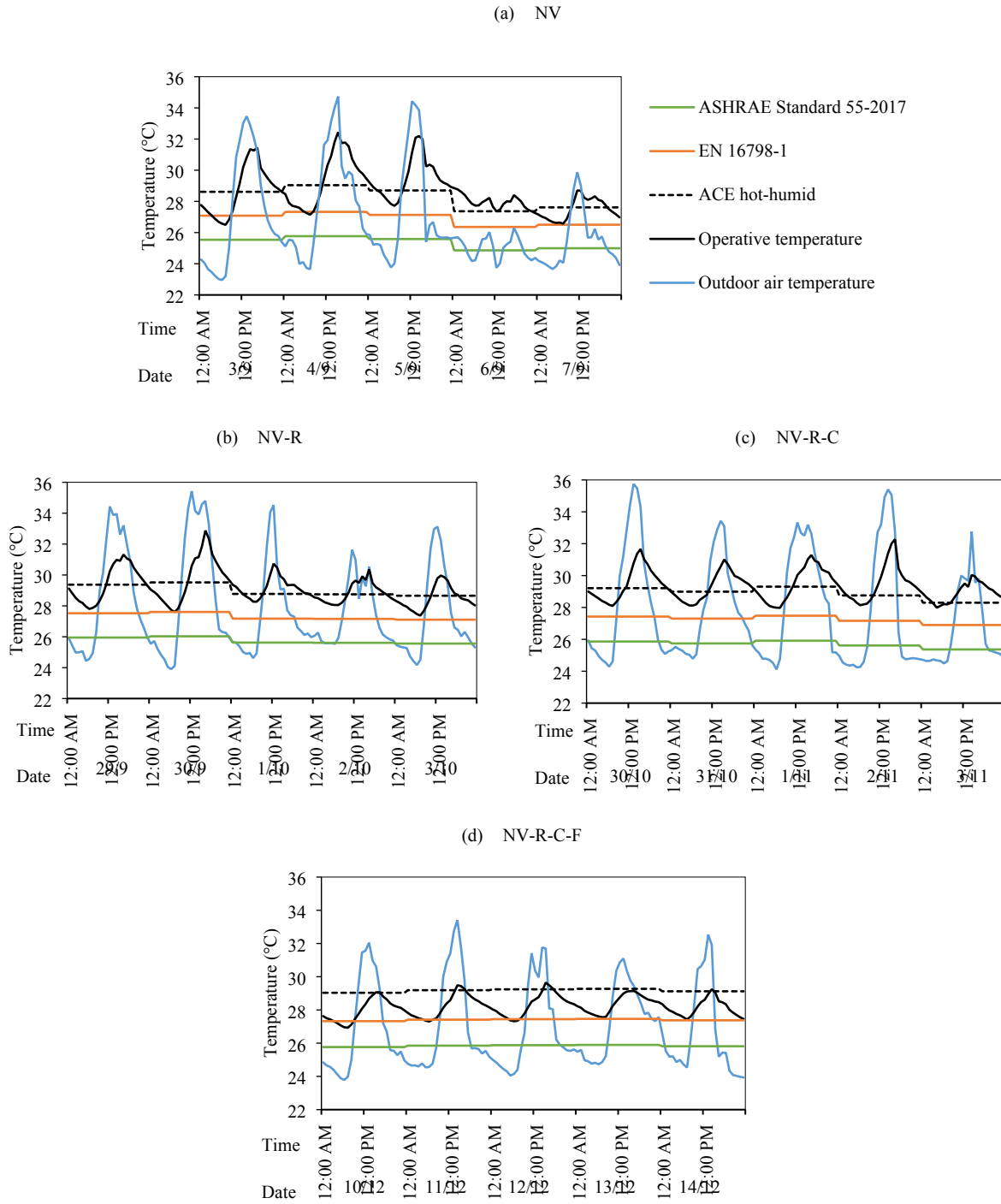


Fig. 19 Relationships between $T_i - T_o$ and T_{eq} .



1 Fig. 20 Comparison of the operative and outdoor air temperatures to the temperatures predicted by related international standards.

Table 1 Characteristics of the investigated house.

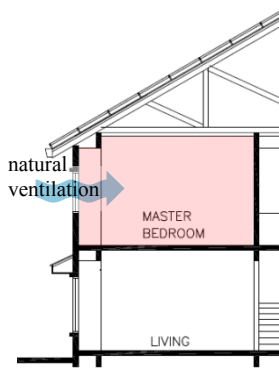
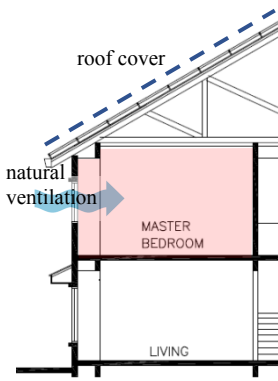
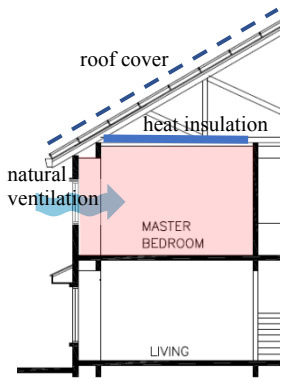
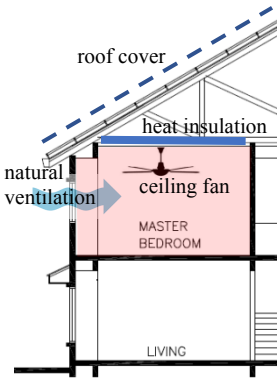
Characteristic	Master bedroom	Bedroom 2	Bedroom 3	Family area	Living area	Dining area
Level	First	First	First	First	Ground	Ground
Orientation of the external wall	West	East	East/South	South	West	South
Floor area (m ²)	15.2	9.6	9.6	16.3	15.2	15.7
External wall area (m ²)	8.1	6.2	16.6	17.7	6.3	9.3
Window area (m ²)	2.9	2.2	3.6	1.5	3.6	1.8
Window-to-wall ratio	0.36	0.35	0.22	-	-	-
External-wall-to-floor ratio	0.53	0.65	1.73	-	-	-

Table 2 Building materials of the investigated house.

Component	Material (structure)	U [W/(m ² ·K)]
Window	Aluminium-frame-fixed single clear glass casement window	5.7 [39]
Door	35-mm-thick solid hardwood panel door	4.9 [38]
Ceiling (first floor)	4.5-mm-thick cement board	66.7 [37]
Wall	114-mm-thick brick wall with 18-mm-thick cement plasters on both sides	3.1 [38]
Floor (ground floor)	150-mm-thick reinforced concrete slab with a 15-mm-thick broken marble finish	0.9 [38]
Floor (first floor)	150-mm-thick reinforced concrete slab with a 5-mm-thick hardwood parquet finish	1.0 [38]
Roof	12-mm-thick concrete roof tile	70.8 [40]
Shading device to window	Canopy roof with concrete roof tiles	–

Note: The U values are based on common building materials in Malaysia [37–40].

Table 3 The four cases of study considered.

Case	NV	NV-R	NV-R-C	NV-R-C-F	
Strategy	Passive cooling	Combination of passive cooling and building retrofitting	Combination of passive cooling and building retrofitting	Combination of passive cooling, building retrofitting and active cooling	
Method	Full day natural ventilation	Full day natural ventilation with a retrofit roof cover	Full day natural ventilation with a roof cover and heat insulation above the ceiling	Full day natural ventilation with a roof cover, heat insulation above the ceiling and mechanical assisted enhanced air movement with a ceiling fan	
<div><div></div><div></div><div></div><div></div></div> <tr><td>Date of measurement</td><td>3/9/2018–7/9/2018</td><td>29/9/2018–3/10/2018</td><td>30/10/2018–3/11/2018</td><td>10/12/2018–14/12/2018</td></tr>	Date of measurement	3/9/2018–7/9/2018	29/9/2018–3/10/2018	30/10/2018–3/11/2018	10/12/2018–14/12/2018
Date of measurement	3/9/2018–7/9/2018	29/9/2018–3/10/2018	30/10/2018–3/11/2018	10/12/2018–14/12/2018	

1

Table 4 Used instruments.

Space	Instrument	Parameter	Manufacturer, country	Sensor type	Resolution	Accuracy and range
Indoor	Thermo-recorder	T_i	Onset, USA	External sensor tmc1-hd	0.03 °C	± 0.35 °C [0 to 50 °C]
	U12-013	T_g		External sensor tmc1-hd + 40-mm black sphere		
		RH_i	Internal sensor	0.05%	± 2.5% (10 to 90%)	
	Hot-wire anemometer	V_i	Kanomax, Japan	Needle probe 6542-2G	0.01 m/s	The larger value between ± 2% of the reading and ± 0.015 m/s
	Data logger GL820	$T_i T_s$		Thermocouple type k		± (0.05% of the reading +1.0 °C)
Outdoor	Thermo-recorder	T_o	Onset, USA	External sensor tmc1-hd	0.03 °C	± 0.35 °C [0 to 50 °C]
	U12-013	RH_o		Internal sensor	0.05%	± 2.5% (10 to 90%)
	Ultrasonic anemometer	V_o	Deltaohm, Italy	Ultrasonic	0.01 m/s	± 0.2 m/s or ± 2% [0 to 35 m/s], ± 2% [>35 m/s]
	HD52.3D					
	Pyranometer CM11	SR	Kipp & Zonen, Netherlands			Sensitivity: 7 to 14 μV/W/m²

2

3

4

Table 5 Average hourly SR values and daily T_o averages for the four cases.

	NV		NV-R		NV-R-C		NV-R-C-F	
	SR (MJ/day)	T_o (°C)	SR (MJ/day)	T_o (°C)	SR (MJ/day)	T_o (°C)	SR (MJ/day)	T_o (°C)
Day 1	17.5	27.2	<u>14.7</u>	28.5	19.5	28.3	10.4	26.8
Day 2	21.6	28.0	10.9	28.8	<u>15.3</u>	27.9	<u>15.1</u>	27.1
Day 3	<u>14.9</u>	27.4	12.1	27.5	15.6	28.4	13.9	26.8
Day 4	4.1	25.0	11.9	27.5	19.5	27.5	10.8	27.4
Day 5	7.9	25.5	11.8	27.3	11.4	26.7	10.3	26.5
Average	13.2	26.6	12.3	27.9	16.2	27.7	12.1	26.9

5

The underlines indicate the days in the different cases having approximately equal SR values.

6

7

1

Table 6 Compliance of operative temperature to ASHRAE55-2017, EN16798-1 and ACE hot-humid for the four cases.

Case	NV	NV-R	NV-R-C	NV-R-C-F
Compliance of T_{op} to ASHRAE Standard 55-2017	No compliance	No compliance	No compliance	No compliance
Compliance of T_{op} to EN 16798-1	No compliance	No compliance	No compliance	13%
Compliance of T_{op} to ACE for hot-humid climate	38%	48%	39%	92%

2